AIP Advances

Modulation of Dirac points and band-gaps in graphene via periodic fullerene adsorption

Xiao Liu, Yanwei Wen, Zhengzheng Chen, Hao Lin, Rong Chen, Kyeongjae Cho, and Bin Shan

Citation: AIP Advances **3**, 052126 (2013); doi: 10.1063/1.4807738
View online: http://dx.doi.org/10.1063/1.4807738
View Table of Contents: http://scitation.aip.org/content/aip/journal/adva/3/5?ver=pdfcov
Published by the AIP Publishing

AIP ADVANCES **3**, 052126 (2013)

Modulation of Dirac points and band-gaps in graphene via periodic fullerene adsorption

Xiao Liu,[1] Yanwei Wen,[1,a] Zhengzheng Chen,[1] Hao Lin,[1] Rong Chen,[2] Kyeongjae Cho,[3] and Bin Shan[1,3,b]

[1]*State Key Laboratory of Material Processing and Die and Mould Technology and School of Materials Science and Engineering, Huazhong University of Science and Technology, Wuhan 430074, Hubei, People's Republic of China*

[2]*State Key Laboratory of Digital Manufacturing Equipment and Technology and School of Mechanical Science and Engineering, Huazhong University of Science and Technology, Wuhan 430074, Hubei, People's Republic of China*

[3]*Department of Materials Science and Engineering, The University of Texas at Dallas, Richardson, Texas 75080, USA*

(Received 30 January 2013; accepted 13 May 2013; published online 20 May 2013)

The structural, energetic and electronic properties of periodic graphene nanobud (PGNB) with small-diameter fullerenes (C_{20}, C_{34}, C_{42}, and C_{60}) adsorbed have been investigated by first-principles plane wave method. The bond-to-ring cycloaddition is found to be energetically most stable among various configurations and the minimum energy paths of different-sized fullerenes attaching to graphene indicate that smaller fullerene shows lower energy barriers due to its larger surface curvature. For perfectly ordered adsorption, band structures analyses by both density functional theory (DFT) and tight binding (TB) methods show that the Dirac cone of graphene can be generally preserved despite the sp^2 to sp^3 bond hybridization change for selected carbon atoms in graphene sheet. However, the position of the Dirac points inside the Brillouin zone has a shift from the hexagonal corner and can be effectively modulated by changing the fullerenes' concentration. For practical applications, we show that a considerable band gap (∼0.35 *eV*) can be opened by inducing randomness in the orientation of the fullerene adsorption and an effective order parameter is identified that correlates well with the magnitude of the band gap opening. [http://dx.doi.org/10.1063/1.4807738]

I. INTRODUCTION

Graphene, a two-dimensional layer with sp^2-bonded carbon atoms on a honeycomb lattice, has aroused great interest for its excellent mechanical, electronic, and chemical properties, since its discovery by mechanical exfoliation of graphite.[1,2] Different from conventional materials, intrinsic graphene is semi-metallic where the valence and conduction bands meet each other at the Dirac point.[3] Dirac point, also known as the topological defect of band structure, is important to the most attractive aspects of graphene, such as a remarkably high electron mobility at room temperature, ballistic transport over micrometer-scale, and anomalous quantum hall effect.[4–7] Many theoretical attempts have been performed to realize topological transition by manipulating Dirac points.[8–10] Very recently, creating and moving Dirac points have been realized in a system of ultracold Fermi gas in a two-dimensional optical lattice.[11] Furthermore, the energy gap in graphene derived structure is another key parameter to describe the band structure, and has technological importance since it determines I_{on}/I_{off} ratios and thus the applicability of graphene in field-effect transistors. It is

[a]Electronic mail: ywwen@mail.hust.edu.cn.
[b]Electronic mail: bshan@mail.hust.edu.cn.

therefore of great importance to achieve effective band structure engineering for graphene. Up to now, a number of approaches have been tried to remedy the zero band gap problem, including bilayer graphene stacking, formation of graphene nanoribbons or graphene antidot lattices, via hetero atom doping, and chemical modification.[12–25] For instance, hybridized h-BNC structures have been synthesized and have a band gap around 18 meV.[19] A gap of ∼0.26 eV can also be produced when graphene is epitaxially grown on a SiC substrate.[25] As for chemical modification method, patterned adsorption of atomic hydrogen onto graphene can lead to band gaps as large as 0.73 eV.[17] Some recent experiments also aim to control Dirac points of graphene. Freitag *et al* achieved the spatial movement of the Dirac point in a biased graphene.[26] Gierz *et al* reported that the Dirac point shifts along energy due to the adsorption of metal atoms.[27] On the other hand, reports on tunable shifting of Dirac points in the momentum space are limited and new methods of controlling Dirac points are needed.

In the present work, we investigate the Dirac points and band gaps of monolayer graphene by covalently bonding fullerenes which can be called periodic graphene nanobud (PGNB).[28,29] In previous studies, the formation of C_{60} attached PGNBs has been reported and is found to be endothermic by 2.80 eV with a high activation barrier of 3.51 eV.[28] We thus focus on small-diameter fullerenes such as C_{20}, C_{34}, and C_{42} which are expected to bond to graphene stronger due to their high activity. Several cycloaddition configurations have been considered and the most stable structure is identified. Band structure analysis shows that perfectly ordered fullerene adsorption leads to shifting of Dirac points without appreciable band gap opening, with the magnitude of shifting correlated to the concentration of adsorbed fullerenes. In contrast, imperfect fullerene adsorption patterns with randomness in the orientation of sp^3 hybridized carbon pairs lead to sizable band gap opening. We further show that the magnitude of the band gap opening can be related to an effective order parameter that describes the relative orientation of hybridized carbon pairs to each other in the graphene lattice.

II. COMPUTATIONAL METHOD

Density functional theory (DFT)[30,31] calculations are performed using the VASP package with projector-augmented-wave (PAW) method[32–34] and the local density approximation (LDA). LDA is chosen because it could improve the structural description of graphitic systems by spuriously mimicking a fraction of the vdW interaction.[35] The wave functions are expanded in a plane wave basis set with an energy cutoff of 400 eV. The $\boldsymbol{k}$ points are sampled on a Monkhorst-Pack[36] grid of $5 \times 5 \times 1$ and the geometry is allowed to relax until Hellmann-Feynman force on each atom is less than 0.05 eV/Å. In order to avoid image interactions, we adopt a hexagonal graphene supercell of 9.84 Å × 9.84 Å and larger, with a vacuum thickness of 20 Å. These settings well reproduce energetic properties and band structures for PGNB systems and is used throughout our study.[36]

III. RESULTS AND DISCUSSIONS

We begin our discussion on the structural stability of differently sized PGNBs. As indicated by statistical measurements of spherical size distribution,[37] C_{60} is the most abundant one among all fullerenes species on carbon nanobuds. Interestingly, those ultra-small fullerenes such as C_{42}, C_{34}, especially the smallest carbon cage C_{20}, were also observed with an appreciable portion in experiments. Geometrically, C_{20} is a symmetric molecule with twelve pentagonal rings, which has been successfully synthetized by chemical dehydrogenation from $C_{20}H_{20}$ and different bulk structures of C_{20} have been obtained.[38–40] Ground state energies of different isomers of C_{34} and C_{42} have also been calculated and the most stable ones are shown in Fig. 1(a), in good agreement with previous studies.[41] Fig. 1(a) shows the supercell of graphene to which fullerenes will be attached. According to the symmetry, fullerenes can bind to graphene via several configurations. Taking C_{20} as an example, four types of cycloadditions are considered (Fig. 1(b)): i) atom-to-atom cycloaddition (**AA**), ii) bond-to-bond cycloaddition (**BB**), iii) bond-to-ring cycloaddition (**BR**), iv) ring-to-ring cycloaddition (**RR**). For C_{34} and C_{42}, there are three types of inequivalent C-C bonds that may get involved in the cycloaddition reaction: C-C bonds shared by a hexagonal and a pentagonal ring

TABLE I. The binding energies of C_{20}-, C_{34}- and C_{42}-PGNBs.

		BB			BR			
Eb (eV)	**AA**	**hh**	**hp**	**pp**	**hh**	**hp**	**Pp**	**RR**
C_{20}	−0.17	/	/	− 0.68	/	/	− 0.91	4.83
C_{34}	/	1.51	1.27	0.70	/	1.18	0.47	5.71
C_{42}	/	1.92	0.87	1.70	/	0.71	1.46	5.68
C_{60}	/	1.86	2.57	/		/		6.42

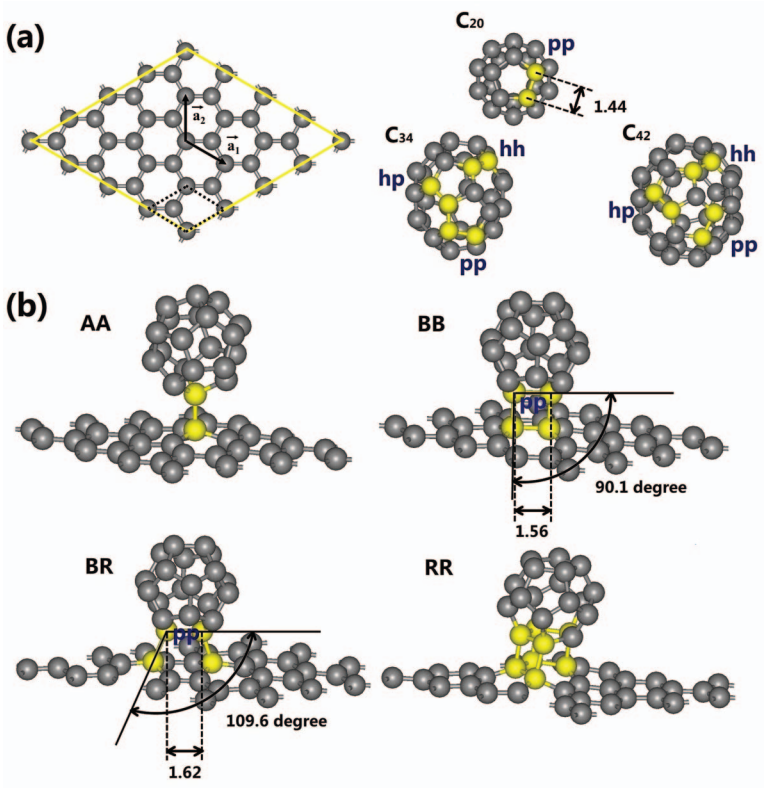

FIG. 1. Optimized structures (a) graphene p(4 × 4) supercell and a single C_{20}, C_{34} and C_{42} molecule. (b) The geometrical structures of C_{20}-PGNB with different cycloaddition configuration(**AA**, **BB**, **BR** and **BR**). The sp^3 hybridized carbon atoms are marked yellow.

(**hp**), by two hexagonal rings (**hh**) and by two pentagonal rings (**pp**). We have considered all the combinations involving these different bonds and cycloadditions, and the lowest energy configuration for each fullerene type was adopted for the subsequent electronic structure analysis.

We have considered all the combinations involving these different cycloadditions and Table I summarizes the calculated binding energies of C_{20}-, C_{34}-, C_{42}-, and C_{60}-PGNBs, which is defined as $E_b = E(\text{PGNB}) - E(\text{graphene}) - E(\text{fullerene})$. Note that more negative value indicates higher stability of the PGNBs. It is clear that binding energies for smaller fullerenes are much lower than that of C_{60}, which can be attributed to their higher curvature and reactivity.[42] The stability across different binding configurations can be qualitatively understood as follows: (a) the primary driving force for the binding is the chemical bond formation. Thus **AA** configuration with one covalent bond is less favorable than **BB** or **BR** configuration with two covalent bonds. As shown in Table I, **BR** cycloaddition is the most stable chemisorption configuration while **AA** is only stable for C_{20}. (b) the binding energy difference for configurations with same number of chemical bonds is primarily due to strain effect. The less favorable binding of **BB** than **BR** can be related to the local structure,

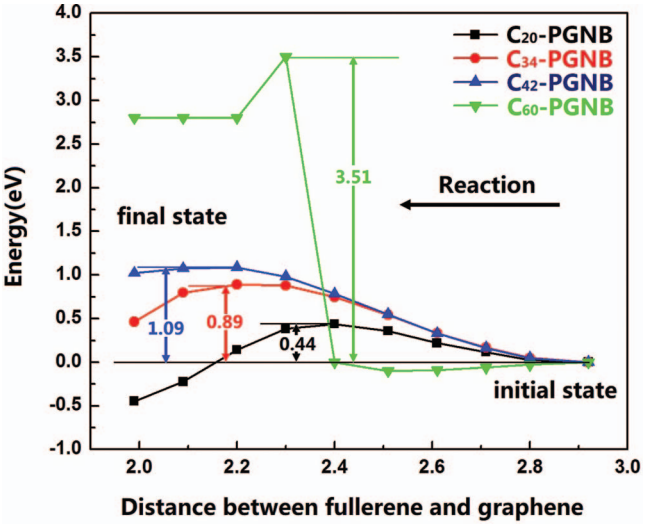

FIG. 2. The estimated minimum energy path for the formation of C_{20}-, C_{34}- and C_{42}-PGNBs (final states) from their stable physisorption states (initial states). The barrier of C_{60}-PGNB (green curve) is also plotted from Ref. 28 for comparison.

where the latter configuration is preferable in releasing the strain caused by sp^3 hybridization in the junction. In **BR** configuration, sp^3 bond angles of the bond-to-ring cycloaddition (Fig. 1(b)) are very close to the ideal tetrahedral angle of 109.5 degree. Meanwhile the bond length of **pp** bond in the fullerene also stretches to 1.62 Å, very close to the bond length of ideal carbon sp^3 bonds. In contrast, the **BB** cycloaddition configuration involves squared carbon ring formation with bond angles of 90 degrees (Fig. 1(b)). This leads to substantial strain and the configuration is thus less stable. For the same reason, ring-to-ring cycloaddition is very energetically unfavorable because of the formation of four squared carbon rings in the junction. As for C_{34} and C_{42}, the binding energies follow the same trend. We notice that binding energies of **BR** cycloadditions show a clear dependence of the fullerenes' size and it becomes less favorable as the size of fullerene increases. This is because the existence of a general repulsion interaction between the non-bonded fullerene and graphene at a distance of ~1.6 Å. Fullerenes with a flatter curvature will cause a stronger repulsion and explains the reduction in adsorption energy going to larger fullerene sizes.

To estimate the energy barriers of PGNBs formation, minimum energy paths (MEPs) for the formation of C_{20}-, C_{34}- and C_{42}-PGNBs have been calculated by the drag method, with results shown in Fig. 2. We choose fullerene molecules in gas phase on graphene monolayer as the initial state and the PGNB as the final state. Eight intermediate images are interpolated linearly with two carbon atoms of C_{20} closest to the graphene kept fixed at the interpolated value and all other degrees of freedom allowed to relax. The distance between fullerene and graphene is taken as the reaction coordinate. For comparison, the barrier of C_{60}-PGNB formation is also plotted. The MEP suggests that the energy barriers for the small-fullerene PGNBs are much lower than that of C_{60}-PGNB (3.51 eV).[28] In particular, the C_{20} attachment barrier is as low as 0.44 eV, about one ninth that of C_{60}-PGNB. The observed smaller barriers are closely related to the sharper curvatures of small fullerenes which facilitates the forward reaction. Note that the reverse reaction, i.e. detachment of C_{20} from PGNB has a relatively high barrier of 0.89 eV, indicating the stableness of C_{20}-PGNB once it is formed.

Since the C_{20}-PGNB is one of the most stable PGNBs, we focus on it in the following discussions. To investigate the change of electronic properties of graphene upon fullerene adsorption, electronic band structure analysis is carried out for C_{20}-PGNB. According to Brillouin zone (BZ) folding rules, two Dirac points K(K') for a pristine graphene folds to $K_4(K_4')$ in a $p(3n+1 \times 3n+1)$ supercell, to $K_5'(K_5)$ in a $p(3n+2 \times 3n+2)$ supercell, and to $K_6 = K_6' = \Gamma$ point in a $p(3n \times 3n)$ supercell as depicted in Fig. 3(a). The band structures of C_{20}-PGNB with a $p(4 \times 4)$, $p(5 \times 5)$ and $p(6 \times 6)$ graphene unit cell are calculated and presented in Fig. 3(c)–3(e). To illustrate the contribution of

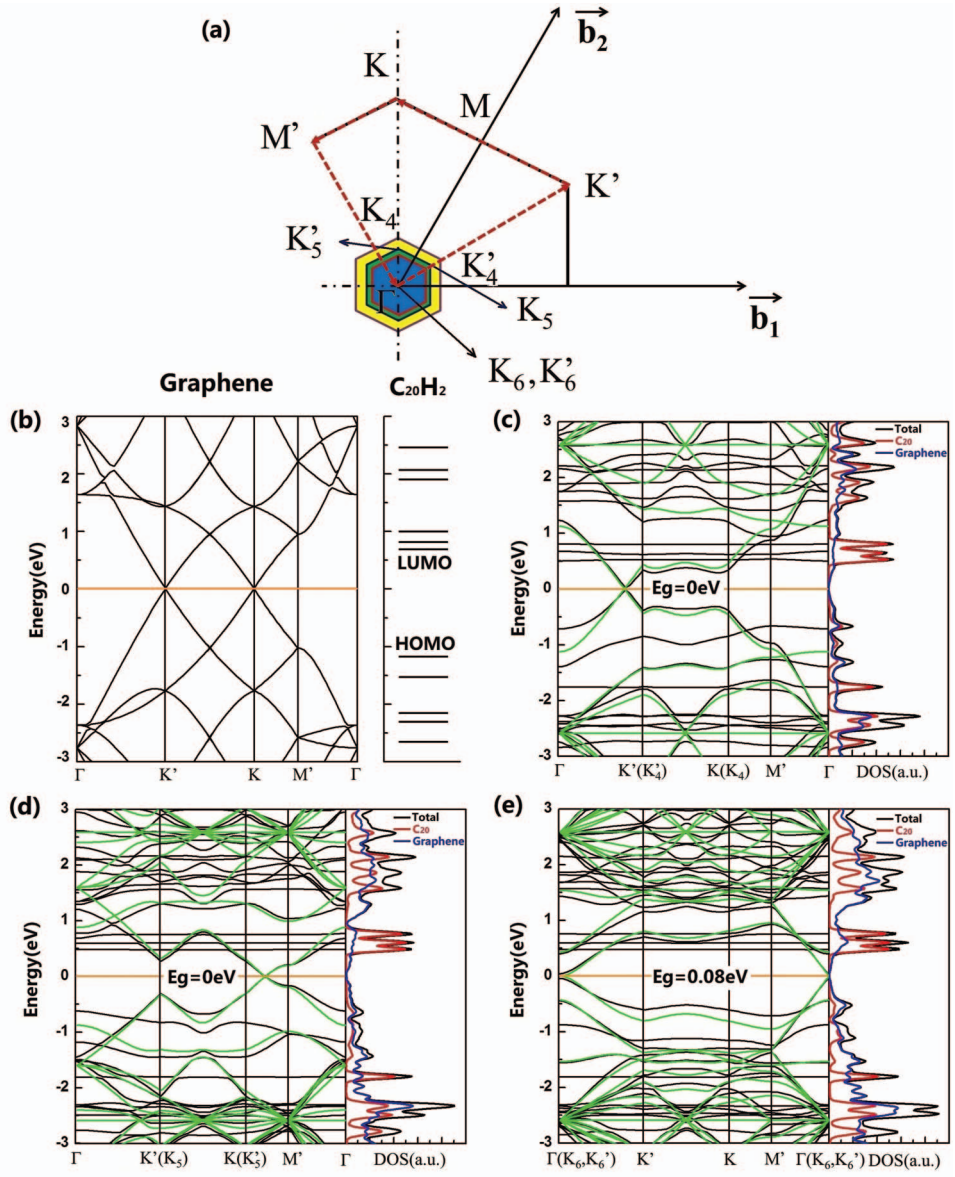

FIG. 3. (a) The first Brillouin zone and high-symmetry K points of the graphene primitive cell, $K_4(K_4')$, $K_5(K_5')$ and $K_6(K_6')$ correspond to the folded K(K') points in a $p(4 \times 4)$, $p(5 \times 5)$ and $p(6 \times 6)$) supercell. (b) The band structure of pristine graphene and the energy level of $C_{20}H_2$ (isolated C_{20} with two atoms passivated by hydrogen atoms). (c-e) The band structure (black line) and DOS of C_{20}-, C_{34}- and C_{42}-PGNB with **BR** cycloaddition in a $p(4 \times 4)$ unit cell based on DFT. The green line is the band structure from π-orbital TB. The total DOS and LDOS of C_{20} and graphene are plotted with black, red and blue lines, respectively.

graphene $p(4 \times 4)$ supercell and fullerene in PGNB, the band structure of graphene and energy level of C_{20} are calculated by DFT. Since the energy level of C_{20} in PGNB would be greatly affected by the two strongly sp^3 hybridized carbon atoms (Fig. 1 **BR** configuration), it is more reasonable to present the energy levels of $C_{20}H_2$ (C_{20} with two atoms passivated by hydrogen) for comparison. The band structure of PGNB can be approximately seen as a topological overlying of those of isolated graphene and $C_{20}H_2$. By comparing the characteristic energy levels near Fermi level of $C_{20}H_2$, such as LUMO and HOMO, we find the positions of energy levels of $C_{20}H_2$ are in good agreement with those appear in PGNB in Fig. 3(b). The topological bands come from graphene can still be clearly distinguished. However, detailed anisotropic changes of band structure have been observed due to the

attaching of C_{20}. We note the band structure of ideal graphene is well kept along the zigzag direction (M'-Γ) and the bands from C_{20} have little dispersion. While along the armchair direction (K'-Γ), serious band splitting occurs in the crossing bands of graphene and C_{20} due to strong hybridization. As a result, the bands of graphene become flattened, indicating a heavier carrier effective mass. These features imply the change of band structures of graphene is closely related to its intrinsic symmetry and the attaching orientation of C_{20} may cause symmetry breaking. In additional, the Dirac point at K' splits a considerable band gap and the energy eigenvalues at points K(M) and K'(M') are no longer equal. We notice that some previous studies focused on the band dispersions along Γ-K-M-Γ only and thus might not yield a complete picture about the defect induced band gaps.[28] In general, there is no guarantee that the gap opening at high symmetric points would not close somewhere else in the BZ. As shown in Fig. 3(b), the PGNB would exhibit a band gap of 0.6 eV along the conventional Γ-K-M-Γ circuit. However, if we include the additional Γ-K_4' segment, band gap diminishes to zero and Dirac cone re-appears. The band structure of C_{20}-PGNB within $p(5 \times 5)$ supercell follows the same trend and the Dirac point appears at K_5'-M_5'. For the case of $p(6 \times 6)$, the Dirac point is located at the Γ point in accordance with BZ folding rule. First-principles calculations reveal the opening of a narrow band gap of about 0.08 eV, similar to the secondary gap in $(3n, 0)$ zigzag nanotubes where n is an integer.[43] For the sake of simplicity, we still regard Γ point as a Dirac point in following discussions. The partial density of states (PDOS) is plotted to identify the contribution of the hybridized bands of PGNB, which is in good agreement with the energy level of isolated $C_{20}H_2$ discussed above. It is found that the bands near the Fermi level have contributions primarily from graphene, with some flat and hybridized C_{20} bands above and below the Fermi level. Since states of C_{20} are relatively far away from the Fermi level, it is expected that the state at the Fermi level is dominated by the π-π^* bands due to p_z orbitals in the graphene, and a π-orbital tight binding (TB) method would capture the essential electronic properties near the Fermi level. Green lines in Fig. 3(b)–3(d) show the TB band structure of PGNBs with p_z hopping integral set to 2.7 eV according to the Tomanek's parameterization scheme.[44] p_z orbitals in the graphene lattice that are directly contacting the fullerene are removed assuming a perfect sp^2 to sp^3 hybridization transition. Comparing to the DFT results, TB well reproduces all the main features of band dispersion near the Fermi level for C_{20}-PGNBs. For brevity, we did not include the band structures for other PGNBs in Fig. 3, but note that the π-π^* bands of C_{34}- and C_{42}-PGNBs near the Fermi level are very similar to that of C_{20}-PGNB. We can thus conclude that the effect of small fullerene adsorption on band structure is approximately equivalent to introducing sp^3 hybridization of corresponding carbon atoms in the graphene lattice. We have also calculated the band structure of C_{34}-, C_{42}-PGNBs and found change of the band structure follows the trend of C_{20}-PGNBs.

It has been shown in many previous studies that graphene band gaps are dependent on the defects patterning[14,17,45,46] and exhibit interesting $3n$-osilation with respect to the supercell size. However, we found that PGNBs can well preserve the Dirac cone regardless of the supercell size, i.e presence of well-ordered sp^3 hybridization pairs (corresponding to **BR** cycloaddition) in the graphene lattice would not open a significant band gap. While a previous study suggests that band gaps would be opened for C_{60} PGNB with **BB** cycloaddition along Γ-M-K-Γ,[28] we found that by taking into account the inequavalent K and K' due to fullerene adsorption, the Dirac point come back in the Γ-K' directions. This is a general feature that we find valid for ordered fullerene adsorption regardless of supercell size. Since the position of Dirac point might deviate from symmetry points in BZ, we have mapped out the conduction band minimum (CBM) and valence band maximum (VBM) of the PGNBs in the entire BZ for $p(4 \times 4)$, $p(5 \times 5)$ and $p(6 \times 6)$ supercell using TB. Fig. 4(a) shows that two Dirac points (D_1 and D_2) can be found in the first BZ for $p(4 \times 4)$ supercell and they are both along the Γ-K' direction in the projection figure (inset). The two Dirac points (D_1, D_2) in the first BZ for $p(5 \times 5)$ supercell are along the M'-K' directions. The Dirac point for $p(6 \times 6)$ coincides with the Γ point. Upon increasing the supercell size, which corresponds to lower concentration of adsorbed fullerenes, the Dirac points of $p(3n + 1 \times 3n + 1)$ and $p(3n + 2 \times 3n + 2)$ series will appear at roughly similar positions, but move toward the K and K' points along the direction marked by black arrows in the insets of Fig. 4(a) and 4(b). $p(3n \times 3n)$ supercell yields a robust Dirac point at Γ. When n is large enough, the intrinsic electronic property of graphene is recovered and Dirac points re-appears at the corresponding K points as predicted by

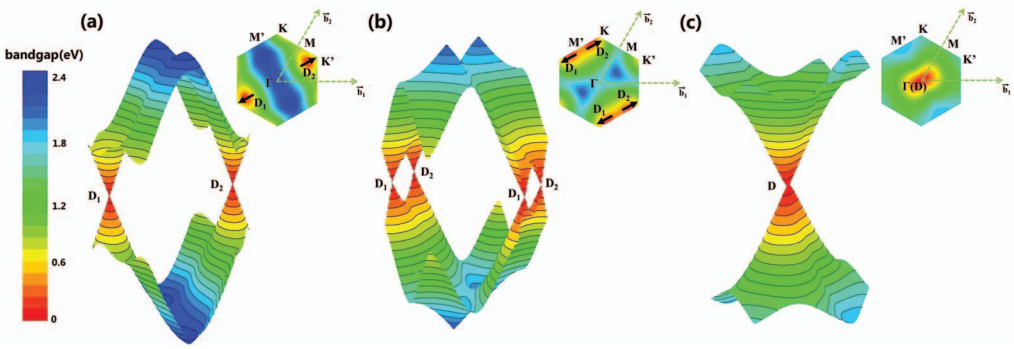

FIG. 4. (a-c) The CBM and VBM states of the PGNBs in $p(4 \times 4)$, $p(5 \times 5)$ and $p(6 \times 6)$ unit cell. The black arrows in (a) and (b) represent the direction which the Dirac points move in when n becomes larger.

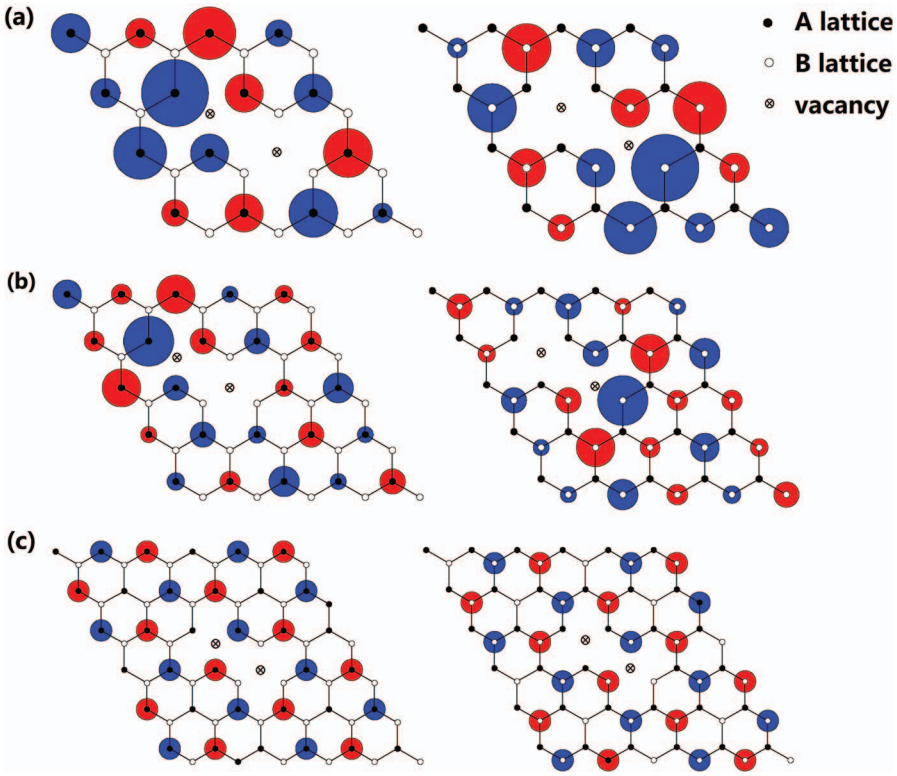

FIG. 5. (a-c) The eigenstates at the Fermi level for $p(4 \times 4)$, $p(5 \times 5)$ and $p(6 \times 6)$ supercell. The red (blue) circles represent positive (negative) component of the wavefunction and the size of the circle corresponds to the wavefunction magnitude.

BZ folding rules. Fig. 4 also indicates that the positions of Dirac points of graphene are predictable and controllable by changing the concentration of fullerene molecules as adsorbates. We note that in general, eigenstates in graphene can be represented by a superposition of A and B sub-lattice states. Fig. 5 plots the spatial distributions of the degenerate A and B sub-lattice states for one of the Dirac points derived from the eigenstates for $p(4 \times 4)$, $p(5 \times 5)$ and $p(6 \times 6)$ supercell. The states at the other Dirac point can be related according to symmetry and are not shown for brevity. The color (red/blue) indicates the sign $(+/-)$ of the wave-function and the radius is proportional to the absolute value of the state. It is not difficult to verify that the wavefunction depicted in Fig. 5 guarantees that it vanishes identically on the sp^3 carbon sites (indicated by circles with cross) at the corresponding K points. For $p(4 \times 4)$ and $p(5 \times 5)$ supercell, the states are localized around the sp^3 carbon sites and show gradual decay moving away from the sp^3 sites. On the other hand, the eigen

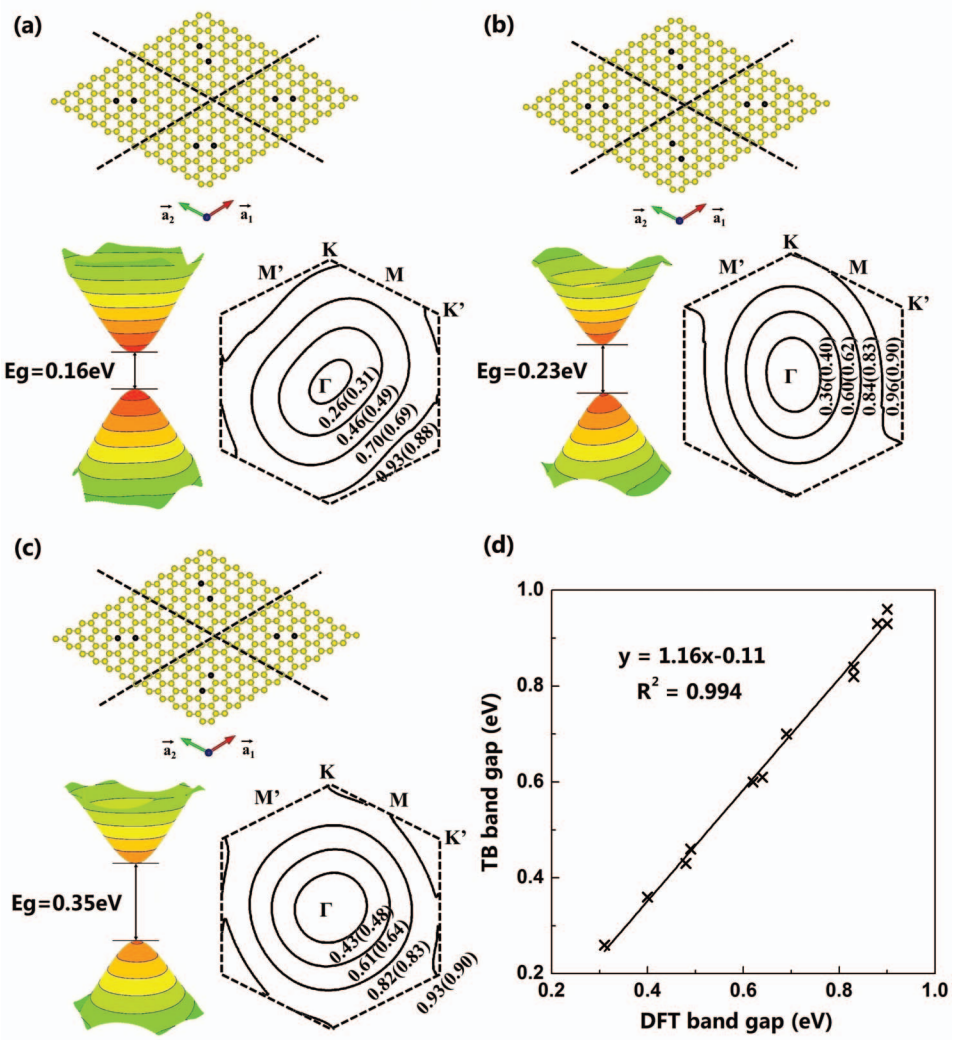

FIG. 6. (a-c) The band gap openings of PGNBs with different orientation randomness in fullerene adsorption. The projection maps represent the CBM and VBM gap in first BZ calculated by both TB and DFT. The values in parenthesis correspond to the band gaps from DFT. Black dots indicate the corresponding sp^3 hybridized carbon pairs in the graphene lattice upon small fullerene adsorption. (d) The linear fitting relationship of the band gaps calculated by TB and DFT in (a-c).

state for $p(6 \times 6)$ is uniformly distributed on both A and B sub-lattice regardless of the distance from the sp^3 sites. This is because in a $p(6 \times 6)$ unit cell, both A and B lattice states happen to vanish on the carbon sites where sp^2 to sp^3 transitions take place, thus there is effectively no perturbation to the original eigen state.

Having shown that there is no appreciable band gap opening in PGNBs with well-ordered **BR** cycloaddition, we further introduced randomness in the fullerene adsorption pattern within the unit cell, which might happen at elevated temperatures or due to external potential perturbations. We choose a relatively large $p(12 \times 12)$ supercell to accommodate the four C_{20}s which might change orientation with respect to each other. For each individual fullerene adsorption, there is a **BR** cycloaddition, which we have shown is electronically equivalent to sp^3 hybridization of a pair of contrapuntal carbon atoms in the graphene lattice. As shown in a previous study, the gap opening due to the adsorption-induced sp^3 bonding is sensitive to the shape, size, and periodicity of adsorbates on graphene.[18] In non-ideal conditions, it is possible that the sp^3 hybridized carbon pairs are not perfectly aligned along the same direction. Fig. 6 shows one such case, where we have a $p(12 \times 12)$ supercell and four adsorbed small fullerene molecules. The black dots show the the sp^3 carbon pairs

that correspond to differently oriented **BR** cycloadditions. When all the pairs are aligned in the same direction, it reduces to a $p(6 \times 6)$ case, where we have shown no significant gap appears (Fig. 4(c)). Going from left to right on Fig. 6 corresponds to increased randomness in adsorption orientation that is characterized by the following order parameter:

$$\lambda = \left\langle \sum_{i=1}^{N} |\cos\theta_i| \right\rangle$$

where N is the number of the nearest ones around each carbon pair and θ_i is the angle between a sp^3 hybridization pair and its nearest ith sp^3 hybridization pair. $\langle\rangle$ denotes average over all sp^3 hybridization pairs in a supercell. Thus the order parameter λ indicates the average alignment of all sp^3 hybridization pairs' order within a supercell. If all the carbon pairs are perfectly aligned, λ equals 1 and represents complete ordering. The level of orientation disorder increases with decreasing λ. The order parameters in Fig. 6(a), 6(b) and 6(c) are calculated to be 0.75, 0.66, and 0.58, respectively. We also calculated the band gaps of the above four configurations in the $p(12 \times 12)$ supercell using TB and found that sizable band gaps are opened. The maximum band gap opening ~0.35 eV occurs at the highest orientation randomness configuration. The band structures contours of C_{20}-PGNB with randomness (Fig. 6(a)–6(c)) by DFT have also been calculated, with its values indicated in the parenthesis near each contour lines. The band gaps in Brillouin zone obtained by TB modeling are similar to DFT results, giving us clue that the origin of the band gap opening upon fullerene adsorption can be attributed to the arrangement of sp^3 hybridized carbon pairs in the graphene lattice. Fig. 6(d) give the linear fitting relationship of band gaps obtained by TB and DFT calculations, the coefficient of determinant ($R^2 = 0.994$) also confirms the reliability of TB modeling. It is interesting to see such a correlation between the orientation of the defects and the size of band gap opening, which to our best knowledge, has not been reported before. Such band gap modulation could potentially be useful in electronic device applications.

IV. CONCLUSION

In conclusion, we systematically studied the structural and electronic properties PGNBs with small-diameter fullerenes. By mapping out the CBM and VBM across the full BZ, we reveal that Dirac cones are preserved for well-ordered fullerene adsorptions, with its deviation from the ideal case correlated to the concentration of fullerene adsorption. Sizable band gaps can be opened by introducing orientation randomness in fullerene adsorption pattern. Our results provide new possible ways of engineering the graphene band structure.

ACKNOWLEDGMENTS

This work is supported by the National Basic Research Program of China (2013CB934800), National Natural Science Foundation of China (Grant 11004068 and 51101064), Fundamental Research Funds for the Central Universities, HUST (2012TS012 and 2012TS076). The authors acknowledge the Thousand Young Talents Plan and New Century Excellent Talents in University (NCET). The calculations are done at the Texas Advanced Computing Center (TACC) at The University of Texas at Austin (http://www.tacc.utexas.edu).

[1] K. S. Novoselov, A. K. Geim, S. V. Morozov, D. Jiang, Y. Zhang, S. V. Dubonos, I. V. Grigorieva, and A. A. Firsov, Science **306**, 666 (2004).
[2] A. K. Geim, Science **324**, 1530 (2009).
[3] A. H. Castro Neto, F. Guinea, N. M. R. Peres, K. S. Novoselov, and A. K. Geim, Rev. Mod. Phys. **81**, 109 (2009).
[4] D. Gunlycke, H. M. Lawler, and C. T. White, Phys. Rev. B **75**, 85418 (2007).
[5] K. S. Novoselov, Z. Jiang, Y. Zhang, S. V. Morozov, H. L. Stormer, U. Zeitler, J. C. Maan, G. S. Boebinger, P. Kim, and A. K. Geim, Science **315**, 1379 (2007).
[6] Y. B. Zhang, Y. W. Tan, H. L. Stormer, and P. Kim, Nature **438**, 201 (2005).
[7] X. Du, I. Skachko, A. Barker, and E. Y. Andrei, Nat. Nanotech. **3**, 491 (2008).
[8] Y. Hasegawa, R. Konno, H. Nakano, and M. Kohmoto, Phys. Rev. B **74**, 033413 (2006).
[9] P. Dietl, F. Piéchon, and G. Montambaux, Phys. Rev. Lett. **100**, 236405 (2008).

[10] S. L. Zhu, B. G. Wang, and L. M. Duan, Phys. Rev. Lett. **98**, 260402 (2007).
[11] L. Tarruell, D. Greif, T. Uehlinger, G. Jotzu, and T. EssLinger, Nature **483**, 302 (2012).
[12] T. Ohta, A. Bostwick, T. Seyller, K. Horn, and E. Rotenberg, Science **313**, 951 (2006).
[13] Y. W. Son, M. L. Cohen, and S. G. Louie, Phys. Rev. Lett. **97**, 216803 (2006).
[14] F. P. Ouyang, S. l. Peng, Z. F. Liu, and Z. R. Liu, ACS Nano **5**, 4023 (2011).
[15] O. U. Akturk and M. Tomak, Appl. Phys. Lett. **96**, 81913 (2010).
[16] H. M. Huang, Z. B. Li, J. C. She, and W. L. Wang, J. Appl. Phys. **111**, 054317 (2012).
[17] R. Balog, B. Jørgensen, L. Nilsson, M. Andersen, E. Rienks, M. Bianchi, M. Fanetti, E. Lægsgaard, A. Baraldi, S. Lizzit, Z. Sljivancanin, F. Besenbacher, B. Hammer, T. G. Pedersen, P. Hofmann, and L. Hornekær, Nature Mater. **9**, 315 (2010).
[18] M. Yang, A. Nurbawono, C. Zhang, Y. P. Feng, and Ariando, Appl. Phys. Lett. **96**, 193115 (2010).
[19] L. J. Ci, L. Song, C. H. Jin, D. Jariwala, D. X. Wu, Y. J. Li, A. Srivastava, Z. F. Wang, K. Storr, L. Balicas, F. Liu, and P. M. Ajayan, Nature Mater. **9**, 430 (2010).
[20] B. S. Pujari, S. Gusarov, M. Brett, and A. Kovalenko, Phys. Rev. B **84**, 041402 (2011).
[21] H. Y. He, Y. Zhang, and B. C. Pan, J. Appl. Phys. **107**, 114322 (2010).
[22] L. Liu and Z. X. Shen, Appl. Phys. Lett. **95**, 252103 (2009).
[23] P. Shemella and S. K. Nayak, Appl. Phys. Lett. **94**, 32101 (2009).
[24] F. Yavari, C. Kritzinger, C. Gaire, L. Song, H. Gullapalli, T. Borca-Tasciuc, P. M. Ajayan, and N. Koratkar, Small **6**, 2535 (2010).
[25] S. Y. Zhou, G. H. Gweon, A. V. Fedorov, P. N. First, W. A. De Heer, D. H. Lee, F. Guinea, A. H. Castro Neto, and A. Lanzara, Nature Mater. **6**, 770 (2007).
[26] M. Freitag, H. Y. Chiu, M. Steiner, V. Perebeinos, and P. Avouris, Nature Nanotech. **5**, 497 (2010).
[27] I. Gierz, C. Riedl, U. Starke, C. R. Ast, and K. Kern, Nano Lett. **8**, 4603 (2008).
[28] X. J. Wu and X. C. Zeng, Nano Lett. **9**, 250 (2008).
[29] E. F. Sheka and L. Kh. Shaymardanova, J. Mater. Chem. **21**, 17128 (2011).
[30] P. Hohenberg and W. Kohn, Physical Review **136**, B864 (1964).
[31] W. Kohn and L. J. Sham, Physical Review **140**, A1133 (1965).
[32] G. Kresse and J. Hafner, Phys. Rev. B **47**, 558 (1993).
[33] G. Kresse and J. Hafner, Phys. Rev. B **49**, 14251 (1994).
[34] G. Kresse and J. Furthmüller, Phys. Rev. B **54**, 11169 (1996).
[35] H. Rydberg, N. Jacobson, P. Hyldgaard, S. I. Simak, B. I. Lundqvist, and D. C. Langreth, Surf. Sci. **532**, 606 (2003).
[36] H. J. Monkhorst and J. D. Pack, Phys. Rev. B **13**, 5188 (1976).
[37] A. G. Nasibulin, P. V. Pikhitsa, H. Jiang, D. P. Brown, A. V. Krasheninnikov, A. S. Anisimov, P. Queipo, A. Moisala, D. Gonzalez, G. Lientschnig, A. Hassanien, S. D. Shandakov, G. Lolli, D. E. Resasco, M. Choi, D. Toma Nek, and E. I. Kauppinen, Nature Nanotech. **2**, 156 (2007).
[38] H. Prinzbach, A. Weiler, P. Landenberger, F. Wahl, J. Wörth, L. T. Scott, M. Gelmont, D. Olevano, and B. V. Issendorff, Nature **407**, 60 (2000).
[39] Z. Iqbal, Y. Zhang, H. Grebel, S. Vijayalakshmi, A. Lahamer, G. Benedek, M. Bernasconi, J. Cariboni, I. Spagnolatti, R. Sharma, F. J. Owens, M. E. Kozlov, K. V. Rao, and M. Muhammed, Eur. Phys. J. B **31**, 509 (2003).
[40] Z. X. Wang, X. Z. Ke, Z. Y. Zhu, F. Y. Zhu, M. L. Ruan, H. Chen, R. B. Huang, and L. S. Zheng, Phys. Lett. A **280**, 351 (2001).
[41] Sun, M. C. Nicklaus, and R. H. Xie, J. Phys. Chem. A **109**, 4617 (2005).
[42] S. Park, D. Srivastava, and K. Cho, Nano Lett. **3**, 1273 (2003).
[43] M. Ouyang, J. L. Huang, C. L. Cheung, and C. M. Lieber, Science **292**,702 (2001).
[44] S. Reich, J. Maultzsch, C. Thomsen, and P. Ordejón, Phys. Rev. B **66**, 035412 (2002).
[45] R. Martinazzo, S. Casolo, and G. F. Tantardini, Phys. Rev. B **81**, 245420 (2010).
[46] S. Casolo, R. Martinazzo, and G. F. Tantardini, J. Phys. Chem. C **115**, 3250 (2011).